Micro-nano-scale Stimulation of Coalbed Methane Reservoir: Experimental Hydraulic Fracturing and Pore Connectivity

Jienan Pan[1], Pengwei Mou[1], Yiwen Ju[2], Kai Wang[1], Taoyuan Ge[1], Qingzhong Zhu[3], Yanhui Yang[3]， Kun Yu[2]， Yanhui Yang[1]

[1] School of Resources & Environment, Henan Polytechnic University, Collaborative Innovation Center of Coalbed Methane and Shale Gas for Central Plains Economic Region, Henan Province, Jiaozuo 454000, China.

[2] Key Laboratory of Computational Geodynamics, College of Earth and Planetary Sciences, University of Chinese Academy of Sciences, Beijing 100049, China.

[3] Coal Bed Methane Pilot Exploitation Test Base of China National Petroleum Corporation, Huabei Oilfield Company, PetroChina, Renqiu 062552, China.

Corresponding author: Jienan Pan and Yuwen Ju

jn_pan@hpu.edu.cn; juyw03@163.com

Key Points:

- This study provided novel and detailed insights into the microscopic mechanisms of coal hydraulic fracturing
- The changes of pore number resulted in the changes of pore volume and specific surface area after hydraulic fracturing
- The change characteristics of coal pore hydraulic fracturing were affected by elastic mod ulus and in-situ stress

Abstract

The role of micro-nano-scale stimulation of coalbed methane (CBM) reservoir is to open the fracture and pore channels, improve gas desorption and migration capabilities, and thereby increase CBM production capacity. Based on hydraulic fracturing simulation experiments, combined with liquid nitrogen absorption (LNA) and mercury intrusion porosity (MIP) measurements, the micro-nano-scale pore structure of coal before and after hydraulic fracturing stimulation in coal reservoirs was studied. It is found that significant changes in the number of pores in different pore sizes are the main reason for the changes in coal pore volume (PV) and pore specific surface area (PSSA) after hydraulic fracturing. the micro-nano-scale pore stimulation of hydraulic fracturing includes two forms of pore fragmentation and pore deformation, the coal with larger elastic modulus is mainly manifested as brittle crush. Moreover, larger in-situ stress will inhibit pore fracture and expansion, and even cause further compression of pores.

Plain Language Summary

The application of hydraulic fracturing technology provides more possibilities for the development of coalbed methane (CBM). Hydraulic fracturing mainly acts on the coal matrix to connect the originally isolated pores and fractures, increasing the development potential of CBM. However, previous studies could not explain the effect of hydraulic fracturing on pores accurately. We have studied the pores of coal after hydraulic fracturing, the research results prove that the number of pores in coal changes significantly after hydraulic fracturing, which causes the redistribution of pores. The change forms of pores after hydraulic fracturing are determined by the elastic modulus of coal, the larger the elastic modulus of coal means that the pores are more easily broken to form smaller pores. However, the phenomenon of pore fragmentation or expansion will be limited as the in-situ stress increases.

1 Introduction

The stimulation of micro-nano-scale pore fissures in low-porosity and low-permeability coalbed methane (CBM) reservoirs can increase the connectivity of micro-nanopore fissure structures in CBM reservoirs, improve the permeability of coal reservoirs, increase the recovery rate of CBM and the production of CBM, and promote the effective development of CBM (Ju et al., 2018). The effective development of CBM is of great significance to alleviate the world energy crisis, reduce the emission of methane from coal mine shafts during coal mining and prevent and control coal mine gas disasters.

China has abundant CBM resources. As a reservoir for the production and occurrence of CBM, the characteristics of the coal seam are important for CBM production. Considering that coal seams usually have a double pore structure (Liu et al., 2011; Liu et al., 2015), the pore structure of coal directly determines the characteristics of gas adsorption, desorption, and diffusion (Pan et al., 2015), which in turn affects the development of CBM. Therefore, the pore development characteristics of coal seams have been a research focus (Clarkson & Bustin, 1999; Zhang et al., 2012). The development of the original pore structure of coal in China is not ideal, the coal seam pore structure is affected by coal pore pressure, effective stress, and matrix deformation (Liu & Harpalani, 2014; Zhou et al., 2016; Liang et al., 2017; Hou et al., 2017; Li et al., 2018), and coal seams in China have strong heterogeneity and low permeability, which is not conducive to CBM production or to the prevention of mine gas disasters. For the efficient development of CBM and for the prevention and control of coal mine gas outbursts, it is imperative to stimulate CBM reservoirs at the micro-nano-scale (Ju et al., 2017), especially for high rank coal reservoirs with more micropores and less fractures.

To improve the efficiency of CBM reservoir stimulation, researchers have proposed various technical approaches, including high-pressure pulsed water jets (Liu et al., 2011), water jet slotting (Shen et al., 2015), enhancement with carbon dioxide injection (CO2-ECBM) (Busch & Gensterblum, 2011; Gensterblum et al., 2014; Fan et al., 2019; Wang et al., 2020), acoustic shocks (Zhang & Li, 2017), microwave vibration (Kumar et al., 2011), and hydraulic fracturing technology (Lu et al., 2020; Tan et al., 2017). Xie et al. (2020) studied the pore structure of coal after pulsating hydraulic fracturing and found that under the action of pulsating hydraulic fracturing, there are two main changes in pores: expansion of original pores and formation of new pores. Cai et al. (2013) conducted heat treatment on coals of different ranks and found that heat treatment could significantly increase the porosity of coal samples. Shi et al. (2016) found that repeated strong pulse waves had a greater impact on coal pore structure, and that smaller pores were more sensitive than larger pores. For the more commonly used hydraulic fracturing technology in the development of CBM, research has mainly focused on macrofractures caused by hydraulic fracturing: The initiation and expansion of hydraulic fractures is mainly affected by reservoir physical properties, horizontal in-situ stress difference, and construction conditions. Hydraulic fracture initiation is mainly controlled by the physical properties of coal reservoirs. Under a constant water pressure, the greater the original permeability, porosity, elastic modulus, and Poisson's ratio of coal, the easier it was for coal to produce hydraulic fractures (Li & Xing, 2015). The extensive development of primitive fractures near the well also reduced the pressure of hydraulic fracture initiation and expansion (Dehghan et al., 2016). The propagation of hydraulic fractures was mainly affected by in-situ stress (Ma et al., 2016; Zhang et al., 2018). Construction conditions (injection pressure, injection rate, fracturing fluid viscosity) have a significant influence on the initiation and expansion of hydraulic fractures (Li et al., 2014). For micro-nano-scale pores, Lu et al. (2020) studied the dynamic evolution of coal pores based on online hydraulic fracturing technology, and found that within 10–120 min of fracturing fluid injection, the total porosity of the coal increased dramatically and pores were formed. As the injection pressure decreases, the number of micropores (< 10 nm) and transition pores (10–100 nm) continued to increase. However, the above-mentioned studies mainly focused on the stimulation of CBM reservoirs at the micro-nano-scale by other stimulation methods. For more commonly used hydraulic fracturing technology, studies have focused on fractures caused by hydraulic fracturing, and there is little research on micro-nano-scale pore hydraulic fracturing stimulation of large-scale coal samples, especially the influence of hydraulic fracturing on nano pores.

In this study, based on mercury intrusion porosity (MIP) and liquid nitrogen absorption (LNA), the changes of coal pore development and pore connectivity before and after hydraulic fracturing were compared, and the mechanism of pore hydraulic fracturing stimulation was analyzed. The conclusions of this study provide guidance for optimizing hydraulic fracturing technology, improving coal seam permeability, increasing CBM production, and for effectively solving mine gas outburst problems.

2 Sample collection and experimental methods

2.1 Characteristics of high-rank coal samples in southern Qinshui Basin

The study area is located in the southern Qinshui Basin of Shanxi Province, China, which is one of the most important CBM industrial development base in China. In order to better study the effect of hydraulic fracturing of high-rank coal pores in Qinshui Basin, anthracite samples from Chengzhuang Mine and Sihe Mine were selected for hydraulic fracture simulation experiments. The mean random vitrinite reflectance of the CZ coal sample was 2.405 and that of the SH coal sample was 2.385.

The mechanical properties of coal is an important factor affecting the crush characteristics of coal hydraulic fracturing. Mechanical properties of coal were measured by uniaxial compression using a KMT-150 rock mechanics experimental system and performed in reference to national standard GB-T23561.1-16-2009 of the People's Republic of China. The elastic modulus of CZ coal samples was 4.206 GPa and Poisson's ratio was 0.223, and these of SH coal samples were 3.432 GPa and 0.297, respectively.

2.2 Hydraulic fracturing simulation experiment

After coal samples were processed, samples SHF-1, SHF-2, and CZF-1 were wrapped with concrete into 300 × 300 × 300 mm sample blocks, owing to its larger volume, sample CZF-2 was wrapped into a block of 400 × 400 × 400 mm. After the concrete had cured for 24 h, each test block was drilled with a rock drill, with vertically layered drilling directions, the diameter of the borehole was ~1 cm to simulate a typical drilling process. The wellbore was put into the hole and then tightly combined with the well wall using epoxy to simulate the cementing process, a space of 3–5 cm was reserved below the wellbore to simulate an open hole section. In this experiment, slickwater (containing 0.5% KCl) with a viscosity of 3 MPa•s was used as the fracturing fluid. Considering the influence of in-situ stress on the experimental results, the in-situ stress of SHF-1 and CZF-1 samples was σ_H: 15 MPa, σ_h: 11 MPa, σ_V: 20 MPa, and that of SHF-2 and CZF-2 samples was set to σ_H: 19 MPa, σ_h: 11 MPa, σ_V: 20 MPa to simulate the stress conditions of the deep coal seam (about 600 m), where σH and σh were horizontal in-situ stress, and σ_V was vertical stress. The specific experimental device and procedure Zhou et al. (2008) have described in detail.

2.3 Measurement and experimental methods of micro-nano pore structure

After completion of hydraulic fracturing experiments, four coal samples were selected in the vicinity of the fracturing wellbore, at the same time, original coal samples of Chengzhuang Mine and Sihe Mine were prepared as the standard. It should be noted that all coal samples were evenly sampled and fully mixed to reduce the influence of coal heterogeneity on the experimental results. Samples were crushed to 3–6 mm and 0.18–0.25 mm, and 10 g from each particle size range was selected and dried to a constant weight at 105℃. MIP experiments were conducted on the coal samples with a diameter range of 3–6 mm using an AutoPore IV 9500 mercury injection instrument with a pressure range of 0.00–228.00 MPa and a test aperture range of 5.5 nm–360 μm. The experimental process was conducted according to standard GB/T21650.1-2008. In addition, LNA experiments were carried out on the coal samples with particle sizes of 0.18–0.25 mm using a TriStar II 3flex automatic PSSA and physical adsorption analyzer, the measured pore size distribution range was 0.35–500.00 nm. The experimental process was conducted with reference to standards GB/T 21650.2-2008 and ISO 15901-2:2006.

3 Results and analysis

3.1. Changes of coal pore before and after hydraulic fracturing

The characteristics and distribution of pores in coal vary widely and it is difficult to determine the multi-scale pore distributions of coal samples using a single experimental method. LNA and MIP are commonly used methods in the study of coal pore structural characteristics (Mastalerz et al., 2012; Li et al., 2012). The combination of LNA and MIP is an effective method for comprehensive and quantitative characterization of coal pore structure. LNA experiments following the BJH method are relatively accurate for pore diameters of < 50 nm, while the MIP method has a large error (coal matrix compression effect) in the range of < 30 nm (Li et al., 1999). For the greatest accuracy, we took 50 nm as the threshold (i.e., for pores of > 50 nm diameter the MIP approach was used, for pores of < 50 nm the LNA approach was used) (Barrett et al., 1951).

The pore size division is very important for the study of pore distribution characteristics, and the targeted pore size division method can clearly reflect the distribution characteristics of pores with different pore sizes. In this study, the Hodot classification scheme was used (Hodot, 1966), with pores divided into micropores (< 10 nm), transition pores (10–100 nm), mesopores (100–1000 nm) and macropores (> 1000 nm).

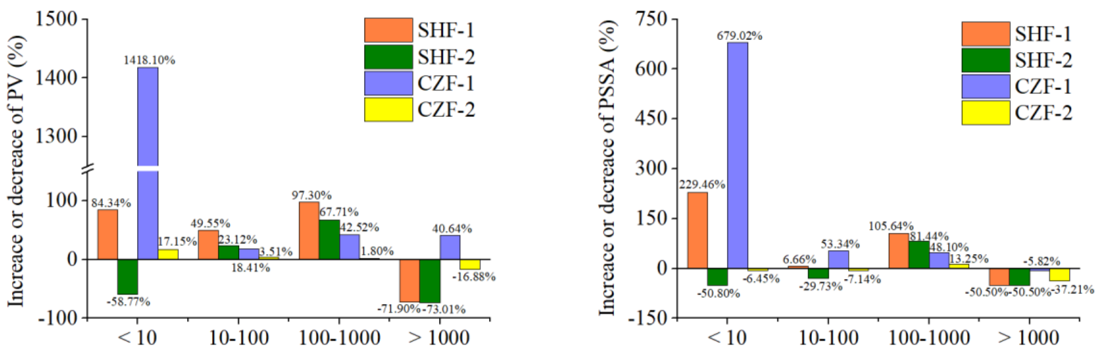

(a) (b)

Figure 1. Variations in the pore volume (PV) and pore specific surface area (PSSA) of coal for different pore sizes ranges before and after hydraulic fracturing experiments. (a): Increase or decrease of PV, (b): Increase or decrease of PSSA.

After hydraulic fracturing, the total PV of coal pores showed a downward trend. Under different in-situ stress conditions, the SHF coal samples of showed the same trend for transition pores, mesopores, and macropores, that is, the volume of transition pores and mesopores increased by varying degrees after hydraulic fracturing (Figure 1a). For micropores, the PV of SHF-1 increased by 84.338% while that of SHF-2 fell by 58.772%. The PV of CZF-1 in the micropores, transition pores and mesopores was the same as that of SHF-1 while that of macropores was the opposite. However, the change trends of CZF-2 were consistent with that of CZF-1 in PV of micropores, transition pores and mesopores, while the change trend of macropores was opposite, the PV of the macropores was reduced by 16.883%. The change amplitude of PV of CZF-2 sample in each aperture section was smaller than that of CZF-1 sample obviously.

The gas adsorption capacity of a coal seam is closely related to the development characteristics of coal PSSA (Clarkson & Bustin, 1999; Ju et al., 2009). After hydraulic fracturing, the total PSSA of coal showed different trends. Compared with the original coal samples (SH: 2.2047 m^2/g, CZ: 0.7356 m^2/g), the total PSSA of SHF-1 (6.5679 m^2/g) and CZF-1 (4.4415 m^2/g) increased significantly, both coal samples showed that PSSA of micropores, transition pores and mesopores increased, while that of macropores decreased (Figure 1b). For the SHF-2 (1.1694 m^2/g) and CZF-2 (0.6904 m^2/g) samples, the total PSSA was reduced 46.960% and 6.141%, respectively, the main manifestations were that the PSSA of micropores, transition pores and macropores were reduced to varying degrees, and the PSSA of mesopores increased significantly.

In general, the change characteristics of PV and PSSA are directly related to the change of pore number. In this study, differential PV versus pore size was used to construct pore size distribution diagrams of coal samples (Figure 2).

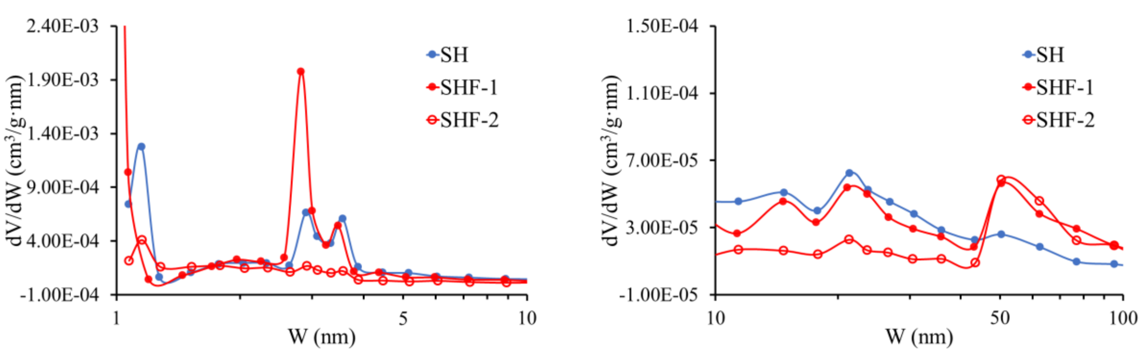

(a) 1–10 nm (b) 10–100 nm

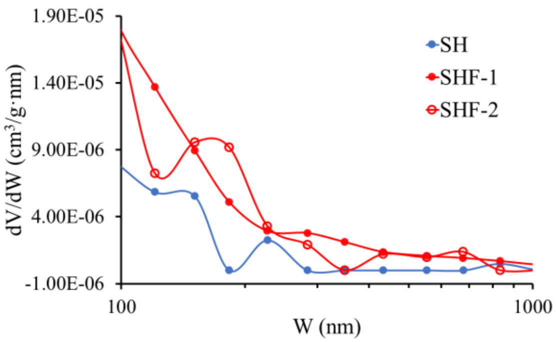

(c) 100–1000 nm

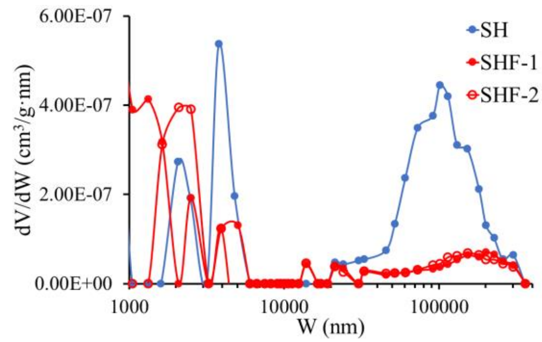

(d) 1000–400000 nm

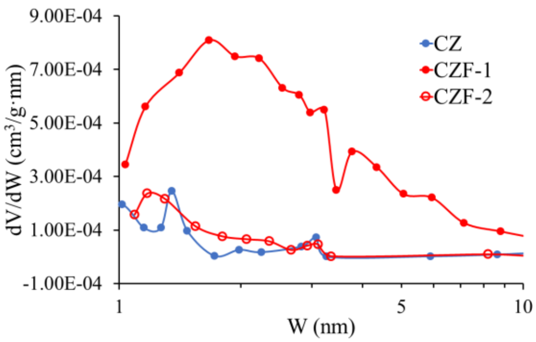

(e) 1–10 nm

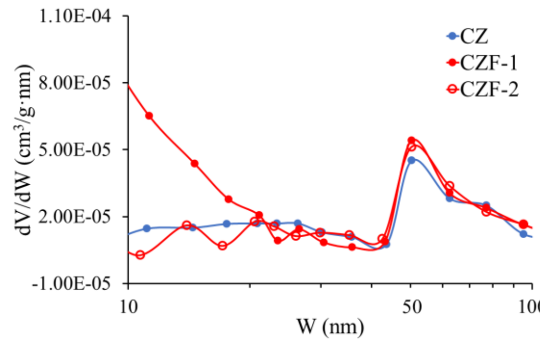

(f) 10–100 nm

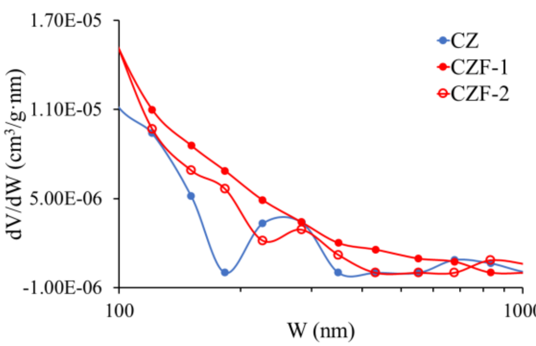

(g) 100–1000 nm

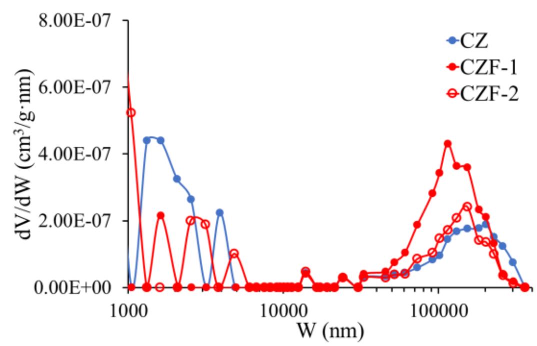

(h) 1000–400000 nm

Figure 2. Distribution of coal pore size before and after hydraulic fracturing experiments. (a), (b), (c) and (d) are pore diameter distribution characteristics of SH samples before and after hydraulic fracturing, (a) 1–10 nm, (b) 10–100 nm, (c) 100–1000 nm, (d) 1000–400000 nm. (e), (f), (g) and (h) are pore diameter distribution characteristics of CZ samples before and after hydraulic fracturing. (e) 1–10 nm, (f) 10–100 nm, (g) 100–1000 nm, (h) 1000–400000 nm.

After hydraulic fracturing, pores changed significantly in the range of 1–100 nm, other aperture segments also had small changes, which could be seen from the order of magnitude of the ordinate in Figure 2. There were differences in the stimulation of different coal samples，this difference was mainly concentrated in the pore size of 1–50 nm and > 1000 nm. The number of micropores in SHF-1 and SHF-2 samples was slightly different from the original coal (SH), the number of pores in most pore segments decreased slightly after hydraulic fracturing, and there was a relatively obvious inflection point within the aperture range between 3–4 nm. CZ ore samples also had obvious inflection points between 3–4 nm, the number of micropores in CZF-1 sample was significantly increased, the CZF-2 sample only began to occupy a smaller advantage in the pore size below 4 nm. After hydraulic fracturing of SH coal, the number of pores in the mesopore section could be divided into two stages: The number of pores in the 50–100 nm aperture section was dominant while the number of pores in the original coal (SH) was more developed in the 10–50 nm aperture section. The CZ samples were more complex, especially the CZF-1 sample, there was a decrease in the number of pores between 20–50 nm, and the number of pores in the pore size range of 10–20 nm and 50–100 nm had an absolute advantage. CZF-2 had a dominant pore size in the 50–100 nm pore size range, but the number of pores was significantly reduced in the 10–50 nm pore size range. The number of macropores of SH coal samples and CZ coal samples showed two opposite trends after hydraulic fracturing: taking 3000 nm as the boundary, the pore number of SHF-1 and SHF-2 samples was dominant at < 3000 nm, and SH pore number was dominant at > 3000 nm. On the contrary, the pore number of CZF samples dominated at > 3000 nm, and CZ sample dominated at 1000–3000 nm pore diameter section. In the mesopore section, the samples after hydraulic fracturing occupied the dominant position.

3.2. Hydraulic fracturing stimulation form of micro-nano-scale pore

From the experimental results, under the same hydraulic fracturing conditions, after hydraulic fracturing of coal samples, the change trends of pore number, PV and PSSA of different samples showed great differences. Considering the different mechanical properties of coal samples, there may be great differences in the form of coal pore stimulation.

Based on the above-mentioned pore change characteristics and connectivity changes of different samples after hydraulic fracturing, it is believed that there are two main forms of pore stimulation during hydraulic fracturing: pore fragmentation and pore deformation (Figure 3), the former mainly occurs in the macropores and mesopores that may be connected during hydraulic fracturing, the latter mainly occurs in transition pores and micropores that are difficult to be connected. The specific form of pore change is also related to the mechanical properties of coal. Considering that SH coal has a larger elastic modulus (4.206 GPa) and a smaller Poisson's ratio (0.223), SH samples were more easily broken with the increase of stress in coal seam. Therefore, in the process of hydraulic fracturing, the macropores and mesopores that could be connected were crushed as the hydraulic pressure in the coal seam gradually increased (Lu et al., 2020), part of them was transformed into microfractures, others was transformed into macropores and mesopores with smaller pore diameters, resulting in a decrease in the number of macropores with a pore diameter > 3000 nm (Figure 2d), while the number of mesoporous segments increased slightly (Figure 2c). On the one hand, the increase in the number of 50–100 nm was caused by the fragmentation of macropores and mesopores. On the other hand, as the pore size range of fracturing fluid could be affected was limited in the process of hydraulic fracturing, fracturing fluid accumulated pressure within the smallest pore size range, and then destroyed this part of the pores, causing a slight increase in the pore size in this range (Figure 2b). In addition, both the expansion of pores and the formation of microfractures required space, it resulted in the compression of some pores and an increase in the number of micropores (Figure 2a) (Shi et al., 2020). As for the decreased in the number of micropores in the SHF-2 sample, it might be related to the in-situ stress conditions.

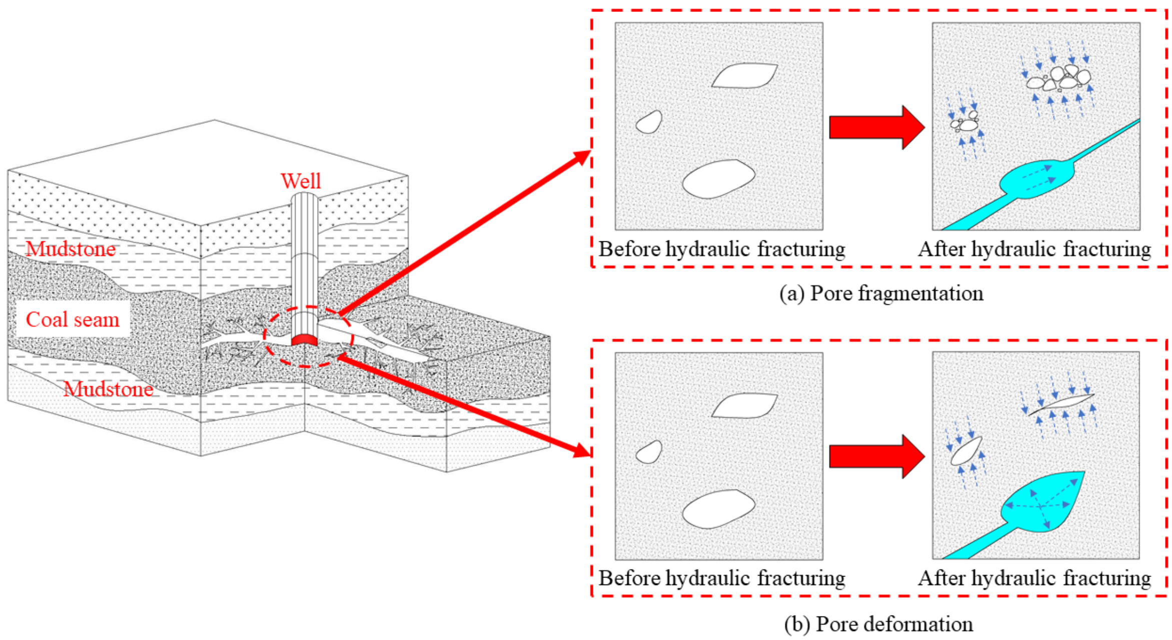

Figure 3. Change model of coal pore structure and connectivity before and after hydraulic fracturing. (a) Pores fragmentation, which mainly includes pores are cut through by fractures and pores are broken into smaller pores. (b) Pore deformation, which mainly includes pore expansion and pore compression. The blue parts in the figures are fracturing fluid.

The CZ coal samples have a smaller elastic modulus (3.432 GPa) and a larger Poisson's ratio (0.297), it means that under the same stress conditions, CZ coal samples are more likely to be squeezed and deformed than SH coal samples (Figure 3b). During the hydraulic fracturing process, as the hydraulic pressure in the coal seam gradually increased, the pores of the CZ coal gradually expanded and deformed. Part of the pores increased to 3000–400000 nm, resulting in an increase in the number of pores in the > 3000 nm (Figure 2h), the other pores continued to expand to reach the crushing strength of CZ coal, which was transformed into microfractures.

Pore expansion compressed the space of pores that cannot be connected, the pores caused by crushing and pore compression were the reasons for the increase in the number of pores in the 50–1000 nm. Similarly, during the hydraulic fracturing process of CZ coal, the pore size range that the fracturing fluid can affect was limited. CZF-1 showed a decrease in the number of pores in 20–50 nm, it might be the minimum pore diameter range that hydraulic fracturing can affect. Under the action of hydraulic pressure, some of the pores in the 20–50 nm expanded, and the pore diameter became larger, at the same time, more pores were compressed, resulting in a sharp increase in the number of pores < 20 nm (Figure 2e and Figure 2f). For CZF-2 sample, the smallest pore size range that can be affected might be smaller (4–50 nm). Part of the 4–50 nm pores expanded, and the pore diameter became larger, resulting in an increase in the number of pores at > 50 nm (Figure 2f), the other pores were compressed, resulting in an increase in the number of pores at < 4 nm (Figure 2e). Obviously, the change in the number of pores in CZF-2 was smaller than that in CZF-1, which might be related to the in-situ stress conditions.

3.3 Coal elastic modulus and coal pore stimulation after hydraulic fracturing

To quantitatively analyze the influence of coal physical properties on hydraulic fracturing, considering that the microscopic material composition of coal and the development of original pore fractures will affect the elastic modulus of coal (Pan et al., 2013), the elastic modulus was chosen as the representative of the physical property of coal reservoir.

With reference to Figure 1, the PV of SHF coal changed drastically, while the PSSA of CZF coal changed drastically after hydraulic fracturing. Considering that SH coal has a larger elastic modulus (4.206 GPa), it is mainly because the greater the elastic modulus, the worse the resistance of coal to deformation under a given pressure, the coal is easily broken during hydraulic fracturing (Li et al., 2012). The crushing of pore will mainly affect the mesopore and macropore with larger scale. The fragmentation and connection of mesopores and macropores increased the pore connectivity of SHF samples, which in turn connected more transition pores and micropores. However, the hydraulic pressure was not enough to have a greater impact on the micropores and transition pores due to the larger elastic modulus of coal. CZ coal has a smaller elastic modulus (3.432 GPa), pore deformation was the main form of hydraulic fracturing micro-nano-scale stimulation of CZ coal, which was mainly manifested in the expansion and compression of pores. In the process of hydraulic fracturing, less pore fragmentation determined that the connectivity between pores had little change. The extension and expansion of microfractures squeezed the pore space, resulting in the tendency of pores to became smaller pores after the formation of hydraulic fractures. Therefore, the PV of micropores of CZF-1 and CZF-2 samples increased after hydraulic fracturing.

In addition, considering that coal has extremely strong heterogeneity (Gibbins et al., 1999; Day et al., 2008; Chen et al., 2013), it cannot be ruled out that the significant increase in macropores PV of CZF-1 was caused by heterogeneity, although the influence of heterogeneity on the experiment was minimized when sampling.

3.4 Influence of in-situ stress on pore stimulation after hydraulic fracturing

The effect of high confining pressure on the fracture of low stiffness results in the rapid decrease of hydraulic aperture, permeability and conductivity (Shu et al., 2020). Similarly, the larger in-situ stress will inhibit the pore crushing and expansion, and even cause the pore further compression.

Considering that the macropores were directly affected by in-situ stress and hydraulic pressure, it was difficult to define the influence of in-situ stress on macropores, the changes of micropores, transition pores and mesopores were strongly affected by in-situ stress. According to Figure 2, it was obvious that under the condition of larger in-situ stress, the number of pores increased less, or even decreased. According to Figure 1, the change ranges of PV and PSSA of micropores, transition pores and mesopores of SHF-1 and CZF-1 samples (σ_H: 15 MPa, σ_h: 11 MPa, σ_V: 20 MPa) were slightly larger than that of SHF-2 and CZF-2 samples (σ_H: 19 MPa, σ_h: 11 MPa, σ_V: 20 MPa) after hydraulic fracturing. Considering that the same coal sample initiation pressure was basically at the same level under different in-situ stress conditions, according to the principle of effective stress, the greater the in-situ stress, the greater the effective stress that the coal will withstand under the similar condition of pore pressure, resulting in the suppression of pores expansion and crushing, and even the compression of pores.

4 Conclusions

In order to find out the influence of hydraulic fracturing on the micro-nano-scale pores of coalbed methane (CBM) reservoirs, which is the core issue for the efficient development of CBM and the prevention of coal mine gas outburst, on the basis of hydraulic fracturing experiments on Chengzhuang (CZ) and Sihe (SH) coal samples, liquid nitrogen absorption and mercury intrusion porosity were used to analyze the pores before and after hydraulic fracturing. It was found that the changes in coal pore volume (PV) and pore specific surface area (PSSA) were caused by changes in the number of pores after hydraulic fracturing, In particular, the number of transition pores and mesopores increased significantly. The changes of pore number, PV and PSSA of micropores and macropores were controlled by the elastic modulus, heterogeneity and in-situ stress conditions of coal: The difference of elastic modulus determines the hydraulic fracturing stimulation form of micro-nano-scale pore. The larger elastic modulus means that coal is dominated by crushing, it is conducive to the improvement of coal pore connectivity under the same in-situ stress conditions. Smaller elastic modulus means that pore deformation is the main factor in the process of hydraulic fracturing. In-situ stress will affect pore crushing, expansion and compression, it is mainly shown that the larger in-situ stress will inhibit the pore crushing and expansion, and even cause the pore further compression.

Acknowledgments

This study was sponsored by the National Natural Science Foundation of China (Grant No. 41772162), the National Science and Technology Major Project of China (2017ZX05064, 2016ZX05066) the Fundamental Research Funds for the Universities of Henan Province (NSFRF180103), the Program for Innovative Research Team of Henan Polytechnic University (T2015-1) and the "Climate Change: Carbon Budget and Related Issues" Strategic Priority Research Program of the Chinese Academy of Sciences (Grant No. XDA05030100).

Data Availability Statement

Data can be found in the Global Change Research Data Publishing and Repository (GCdataPR) at http://www.geodoi.ac.cn/WebEn/doi.aspx?Id=1616

References

Barrett, E. P., Joyner, L. G., & Halenda, P. P. (1951). The Determination of PV and Area Distributions in Porous Substances. I. Computations from Nitrogen Isotherms. Journal of the American Chemical Society, 73(1), 373–380.

Busch, A., & Gensterblum, Y. (2011). CBM and CO2-ECBM related sorption processes in coal: A review. International Journal of Coal Geology, 87(2), 49–71.

Cai, Y. D., Liu, D. M., Pan, Z. J., Yao, Y. B., Li, J. Q., & Qiu, Y. K. (2013). Petrophysical characterization of Chinese coal cores with heat treatment by nuclear magnetic resonance. Fuel, 108, 292–302.

Chen, Z. W., Liu, J. S., Elsworth, D., Pan, Z. J., & Wang, S. G. (2013). Roles of coal heterogeneity on evolution of coal permeability under unconstrained boundary conditions. Journal of Natural Gas Science and Engineering, 15, 38–52.

Clarkson, C. R., & Bustin, R. M. (1999). The effect of pore structure and gas pressure upon the transport properties of coal: a laboratory and modeling study. 1. Isotherms and PV distributions. Fuel, 78(11), 1333–1344.

Day, S., Fry, R., & Sakurovs, R. (2008). Swelling of Australian coals in supercritical CO2. International Journal of Coal Geology, 74(1), 41–52.

Dehghan, A. N., Goshtasbi, K., Ahangari, K., & Jin, Y. (2016). Mechanism of fracture initiation and propagation using a tri-axial hydraulic fracturing test system in naturally fractured reservoirs. European Journal of Environmental and Civil Engineering, 20(5), 560–585.

Fan, C. J., Elsworth, D., Li, S., Zhou, L. J., Yang, Z. H., & Song, Y. (2019). Thermo-hydro-mechanical-chemical couplings controlling CH4 production and CO2 sequestration in enhanced coalbed methane recovery. Energy, 173, 1054-1077.

Gensterblum, Y., Merkel, A., Busch, A., Krooss, B. M., & Littke, R. (2014). Gas saturation and CO2 enhancement potential of coalbed methane reservoirs as a function of depth. AAPG Bull, 98(2), 395–420.

Gibbins, J. R., Beeley, T. J., Crelling, J. C., Scott, A. C., Skorupska, N. M., & Williamson, J. (1999) Observations of Heterogeneity in Large Pulverized Coal Particles. Energy & Fuels, 13(3), 592–601.

Hodot, B. B. (1966). Outburst of Coal and Coalbed Gas (Chinese Translation). Beijing: China Industry Press, p. 318.

Hou, S. H., Wang, X. M., Wang, X. J., Yuan, Y. D., Pan, S. D., & Wang, X. M. (2017). Pore structure characterization of low volatile bituminous coals with different particle size and tectonic deformation using low pressure gas adsorption. International Journal of Coal Geology, 183, 1–13.

Ju, Y. W., Huang, C., Sun, Y., Wan, Q., Lu, X. C., Lu, S. F., et al. (2017). Nanogeosciences: Research history, current status, and development trends. Journal of Nanoscience and Nanotechnology, 17(9), 5930–5965.

Ju, Y. W., Huang, C., Sun, Y., Zou, C. N., He, H. P., Wan, Q., et al. (2018). Nanogeology in China: A review. China Geology, 1, 286-303.

Ju, Y. W., Jiang, B., Hou, Q. L., Tan, Y. J., Wang, G. L., & Xiao, W. J. (2009). Behavior and mechanism of the adsorption/desorption of tectonically deformed coals. Chinese Science Bulletin, 54(1), 88-94.

Kumar, H., Lester, E., Kingman, S., Bourne, R., Avila, C., Jones, A., et al. (2011). Inducing fractures and increasing cleat apertures in a bituminous coal under isotropic stress via application of microwave energy. International Journal of Coal Geology, 88(1), 75–82.

Li, C. W., Xie, B. J., Yang, W., & Wei, S. Y. (2012). Characteristics of Transient Magnetic Nearby Field in Process of Coal Impact Damage. Chinese Journal of Rock Mechanics and Engineering, 31(05), 973–981.

Li, D. Q., Zhang, S. C., & Zhang, S. A. (2014). Experimental and numerical simulation study on fracturing through interlayer to coal seam. Journal of Natural Gas Science and Engineering, 21, 386–396.

Li, Q. S., & Xing, H. L. (2015). Numerical analysis of the material parameter effects on the initiation of hydraulic fracture in a near wellbore region. Journal of Natural Gas Science and Engineering, 27, 1597–1608.

Li, S., Tang, D. Z., Xu, H., & Yang, Z. (2012). The pore-fracture system properties of coalbed methane reservoirs in the Panguan Syncline, Guizhou, China. Geoscience Frontiers, 3(6), 853–862.

Li, X. C., Kang, Y. L., & Haghighi, M. (2018). Investigation of pore size distributions of coals with different structures by nuclear magnetic resonance (NMR) and mercury intrusion porosimetry (MIP). Measurement, 116, 122–128.

Li, Y. H., Lu, G. Q., & Rudolph, V. (1999). Compressibility and Fractal Dimension of Fine Coal Particles in Relation to Pore Structure Characterisation Using Mercury Porosimetry. Particle & Particle Systems Characterization, 16(1), 25–31.

Liang, M. L., Wang, Z. X., Gao, L., Li, C. L., & Li, H. J. (2017). Evolution of pore structure in gas shale related to structural deformation. Fuel, 197, 310–319.

Liu, J. C., Wang, H. T., Yuan, Z. G., & Fan, X. G. (2011). Experimental Study of Pre-splitting Blasting Enhancing Pre-drainage Rate of Low Permeability Heading Face. Procedia Engineering, 26, 818–823.

Liu, J. S., Chen, Z. W., Elsworth, D., Qu, H. Y., & Chen, D. (2011). Interactions of multiple processes during CBM extraction: A critical review. International Journal of Coal Geology, 87(3-4), 175–189.

Liu, Q. Q., Cheng, Y. P., Zhou, H. X., Guo, P. K., An, F. H., & Chen, H. D. (2015). A Mathematical Model of Coupled Gas Flow and Coal Deformation with Gas Diffusion and Klinkenberg Effects. Rock Mechanics and Rock Engineering, 48(3), 1163–1180.

Liu, S. M., & Harpalani, S. (2014). Determination of the Effective Stress Law for Deformation in Coalbed Methane Reservoirs. Rock Mechanics and Rock Engineering, 47(5), 1809–1820.

Lu, Y. Y., Wang, L., Ge, Z. L,. Zhou, Z., Deng, K., & Zuo, S. J. (2020). Fracture and pore structure dynamic evolution of coals during hydraulic fracturing. Fuel, 259, 116272.

Ma, S., Guo, J. C., Li, L. C., Xia, Y. J., & Yang, T. (2016). Experimental and numerical study on fracture propagation near open-hole horizontal well under hydraulic pressure. European Journal of Environmental and Civil Engineering, 20(4), 412–430.

Mastalerz, M., He, L. L., Melnichenko, Y. B., & Rupp, J. A. (2012). Porosity of Coal and Shale: Insights from Gas Adsorption and SANS/USANS Techniques. Energy & Fuels, 26(8), 5109–5120.

Pan, J. N., Meng, Z. P., Hou, Q. L., Ju, Y. W., & Cao, Y. X. (2013). Coal strength and Young's modulus related to coal rank, compressional velocity and maceral composition. Journal of Structural Geology, 54, 129–135.

Pan, J. N., Zhu, H. T., Hou, Q. L., Wang, H. C., & Wang, S. (2015). Macromolecular and pore structures of Chinese tectonically deformed coal studied by atomic force microscopy. Fuel, 139, 94–101.

Shen, C. M., Lin, B. Q., Sun, C., Zhang, Q. Z., & Li, Q. Z. (2015). Analysis of the stress–permeability coupling property in water jet slotting coal and its impact on methane drainage. Journal of Petroleum Science and Engineering, 126, 231–241.

Shi, Q. M., Qin, Y., Li, H. L., Qiu, A. C., Zhang, Y. M., & Zhou, X. T., et al. (2016). Response of pores in coal to repeated strong impulse waves. Journal of Natural Gas Science and Engineering, 34, 298–304.

Shi, R., Liu, J. S., Wang, X. M., Elsworth, D., Liu, Z. H., Wei, M. Y., et al. (2020). Experimental observations of heterogeneous strains inside a dual porosity sample under the influence of gas-sorption: A case study of fractured coal. International Journal of Coal Geology, 223, 103450.

Shu, B., Zhu, R. J., Elsworth, D., Dick, J., Liu, S., Tan, J. Q., et al. (2020). Effect of temperature and confining pressure on the evolution of hydraulic and heat transfer properties of geothermal fracture in granite. Applied Energy, 272, 115290.

Tan, P., Jin, Y., Hou, B., Han, K., Zhou, Y. C., & Meng, S. Z. (2017). Experimental investigation on fracture initiation and non-planar propagation of hydraulic fractures in coal seams. Petroleum Exploration and Development Online, 44(3), 470-476.

Wang, K., Pan, J. N., Wang, E. Y., Hou, Q. L., Yang, Y. H., & Wang, X. L. (2020). Potential impact of CO2 injection into coal matrix in molecular terms. Chemical Engineering Journal, 401, 126071.

Xie, J. N., Xie, J., Ni, G. H., Rahman, S., Sun, Q., & Wang, H. (2020). Effects of pulse wave on the variation of coal pore structure in pulsating hydraulic fracturing process of coal seam. Fuel, 264, 116906.

Zhang, D. F., Gu, L. L., Li, S. G., Lian, P. C., & Tao, J. (2012). Interactions of Supercritical CO2 with Coal. Energy & Fuels, 27(1), 387–393.

Zhang, J. W., & Li, Y. L. (2017). Ultrasonic vibrations and coal permeability: Laboratory experimental investigations and numerical simulations. International Journal of Mining Science and Technology, 27(2), 221–228.

Zhang, Y. S., Zhang, J. C., Yuan, B., & Yin, S. X. (2018). In-situ stresses controlling hydraulic fracture propagation and fracture breakdown pressure. Journal of Petroleum Science and Engineering, 164, 164-173.

Zhou, J., Chen, M., Jin, Y., & Zhang, G. Q. (2008). Analysis of fracture propagation behavior and fracture geometry using a tri-axial fracturing system in naturally fractured reservoirs. International Journal of Rock Mechanics and Mining Sciences, 45(7), 1143–1152.

Zhou, S. D., Liu, D. M., Cai, Y. D., & Yao, Y. B. (2016). Fractal characterization of pore–fracture in low-rank coals using a low-field NMR relaxation method. Fuel, 181, 218–226.